

Estimation-aware model predictive path-following control for a general 2-trailer with a car-like tractor

Oskar Ljungqvist¹, Daniel Axehill¹, Henrik Pettersson², Johan Löfberg¹

¹Department of Automatic Control, Linköping University, Linköping, Sweden.

E-mail: {oskar.ljungqvist, daniel.axehill, johan.lofberg}@liu.se.

² Scania CV, Södertälje, Sweden.

E-mail: henrik.x.pettersson@scania.com.

Abstract

The design of the path-following controller is crucial for reliable autonomous vehicle operation. This design problem is especially challenging for a general 2-trailer with a car-like tractor due to the vehicle's unstable joint-angle kinematics in backward motion. Additionally, advanced sensors placed in the rear of the tractor have been proposed to solve the joint-angle estimation problem. Since these sensors typically have a limited field of view, the estimation solution introduces restrictions on the joint-angle configurations that can be estimated with high accuracy. To explicitly consider these constraints in the controller, a model predictive path-following control approach is proposed. Two approaches with different computation complexity and performance are presented. In the first approach, the joint-angle constraints are modeled as a union of convex polytopes, making it necessary to incorporate binary decision variables. The second approach avoids binary variables at the expense of a more conservative controller. In simulations and field experiments, the performance of the proposed path-following control approach is compared with a previously proposed control strategy.

1 Introduction

Autonomous transport solutions and advanced driver assistance systems are experiencing massive interest in order to increase efficiency and safety, and to reduce the environmental impact related to freight transport. Today, autonomous driving in urban areas still faces many unsolved problems and legislation changes are needed to drive autonomously on public roads. In contrast, autonomous driving in closed areas such as mines and harbors are predicted to be more suitable

for initial deployment of such systems. Within these sites, different tractor-trailer combinations are frequently used for transportation of goods. These vehicles are composed of a car-like tractor and several passive trailers that are interconnected through hitches that are of off-axle or on-axle type. When the connections are of mixed hitching types, the tractor-trailer vehicle is called a general N-trailer (GNT) and when only pure on-axle hitching is present, it is referred to as a standard N-trailer (SNT). Due to the specific kinematic properties of tractor-trailer vehicles [1, 35, 45], the feedback-control problem is in general very difficult. The feedback-control problems that have been investigated in the literature for various tractor-trailer combinations are mainly path following (see e.g., [2, 3, 5, 8, 25, 30, 34, 37, 40, 42, 43, 46]), and trajectory tracking and set-point stabilization (see e.g., [10, 21, 22, 31, 36, 39]). Additionally, to aid human drivers when reversing several advanced drivers-assistance systems concepts have been proposed (see e.g., [7, 12, 18, 32, 33]).

Most of the control approaches presented in the literature address the problem of tracking a geometric trajectory or path defined in the position and orientation of the last trailer's axle. In this work, the path-following control problem during low-speed maneuvers for a full-scale G2T with a car-like tractor (see Figure 1) is considered for the case when the nominal path contains full state and control information, i.e., it is designed to operate in series with a motion planner as in [11, 23, 27]. In such an architecture, it is crucial that all nominal vehicle states are followed to avoid collision with surrounding obstacles.

The feedback-control problem considered in this work is challenging due to the tractor-trailer vehicle's structurally unstable joint-angle kinematics in backward motion and the tractor's limited curvature and curvature rate. Thus, if the vehicle is not accurately steered, these system properties can cause the vehicle segments to fold and enter a jackknife state. Additionally, nonlinear observers together with advanced sensors such as cameras, LIDARs or RADARs mounted in the rear of the car-like tractor have been proposed to solve the problem of estimating the trailer pose and the joint angles [4, 9, 27, 38, 44]. These solutions are promising because the system becomes independent of any trailer sensor. However, because such sensors typically have a limited field of view (FOV), it is important that the vehicle is controlled such that its joint angles remain in the region where high-accuracy state estimates can be computed by the used estimation solution.

The contribution of this work is a path-following control approach for a G2T with a car-like tractor where the vehicle's physical constraints and the rear-view sensor's sensing limitations are modeled and incorporated as constraints in the controller. It is done by proposing a path-following control approach that is based on the framework of model predictive control (MPC) [13, 14, 16, 24, 29].

A preliminary version of the framework has been presented in [26]. Although the controller in [26] is shown to yield a significant performance enhancement compared to previous works,



Figure 1: The test vehicle that is used as research platform. The tractor is a modified version of a Scania R580 6x4, whereas the semitrailer nor the dolly is equipped with any sensor.

it is restricted to only use a single convex polytope to model the joint-angle constraints. On the expense of a conservative controller, the resulting MPC formulation could in our preliminary version be represented as a quadratic programming (QP) problem. However, due to the nonlinear mapping from the rear-view sensor's FOV to the joint-angle space, the allowed joint-angle region may in many applications become non-convex [26]. To alleviate the controller's conservativeness and thus enhance its performance, our previously presented preliminary results are in this work extended by a more complex modeling of the constraints on the joint angles as a union of convex polytopes, where a single polytope as in our previous work is a special case. By incorporating binary decision variables together with big-M modeling strategies [47], the proposed extension results in an MPC formulation that can be cast as a mixed-integer quadratic programming (MIQP) problem. The extension significantly extends the usefulness of the method to even more advanced sensors.

The performance and computation complexity of the proposed MPC approaches are evaluated in a simulation campaign. In the simulations and in field experiments on the full-scale test vehicle shown in Fig. 1, the performance of the proposed predictive path-following control approach in terms of suppressing disturbances and recovering from nontrivial initial states, is compared to the proposed path-following controller in [27] where the vehicle's physical constraints and the estimation solution's sensing-limitations are neglected.

The remainder of the paper is organized as follows. In Section 2, the path-following error model is derived and in Section 3, the proposed MPC approach is presented. The control design as well as the modeling of the vehicle's physical and sensing limiting constraints are presented in Section 4. Results from simulations and field experiments on a full-scale test vehicle are presented in Section 5. Finally, the paper is concluded in Section 6 by summarizing the contributions and a discussion of directions for future work.

2 Vehicle model

The G2T with a car-like tractor is schematically illustrated in Figure 2. The vehicle is composed of three interconnected vehicle segments including a car-like tractor, a dolly and a semitrailer. It is assumed that the vehicle has an off-axle hitch connection between the car-like tractor and the dolly, and an on-axle connection between the dolly and the semitrailer. The state vector $x = [x_3 \ y_3 \ \theta_3 \ \beta_3 \ \beta_2]^T$ is used to represent a configuration of the vehicle, where (x_3, y_3) is the position of the center of the semitrailer's axle, θ_3 is the orientation of the semitrailer, β_3 is the joint angle between the semitrailer and the dolly, and β_2 is the joint angle between the dolly and the car-like tractor. The length L_3 represents the distance between the semitrailer's axle and the dolly's axle, L_2 is the distance between the dolly's axle and the off-axle hitching connection at the car-like tractor, M_1 is the signed hitching offset at the tractor (positive in Figure 2), and L_1 denotes the wheelbase of the car-like tractor. The car-like tractor is assumed to be front-wheeled steered with perfect Ackermann steering geometry, where α denotes its steering angle. The control inputs are the car-like tractor's curvature $u = \frac{\tan \alpha}{L_1}$ and the longitudinal velocity v of its rear axle. Since low-speed maneuvers are considered, a kinematic model is used to describe the vehicle. The model has been presented in, e.g., [3, 27] and is derived based on various assumptions including rolling without slipping of the wheels and that the vehicle is operating on a flat surface. The kinematic vehicle model is given by

$$\dot{x}_3 = v_3 \cos \theta_3, \quad (1a)$$

$$\dot{y}_3 = v_3 \sin \theta_3, \quad (1b)$$

$$\dot{\theta}_3 = v_3 \frac{\tan \beta_3}{L_3}, \quad (1c)$$

$$\dot{\beta}_3 = v_3 \left(\frac{\sin \beta_2 - M_1 \cos \beta_2 u}{L_2 C_1(\beta_2, \beta_3, u)} - \frac{\tan \beta_3}{L_3} \right), \quad (1d)$$

$$\dot{\beta}_2 = v_3 \left(\frac{u - \frac{\sin \beta_2}{L_2} + \frac{M_1}{L_2} \cos \beta_2 u}{C_1(\beta_2, \beta_3, u)} \right), \quad (1e)$$

where $C_1(\beta_2, \beta_3, u)$ is defined as

$$C_1(\beta_2, \beta_3, u) = \cos \beta_3 (\cos \beta_2 + M_1 \sin \beta_2 u), \quad (2)$$

which describes the relationship, $v_3 = v C_1(\beta_2, \beta_3, u)$, between the longitudinal velocity of the semitrailer's axle, v_3 , and the velocity of the car-like tractor's rear axle, v . When $C_1(\beta_2, \beta_3, u) = 0$, the system in (1) is singular [1] and therefore fundamentally difficult to control. It is therefore further assumed that $C_1(\beta_2, \beta_3, u) > 0$.

The model in (1) is compactly represented as $\dot{x} = v_3 f(x, u)$. Since v_3 enters bilinear in (1), time-scaling [27, 41] can be applied to eliminate the longitudinal speed dependence and it is

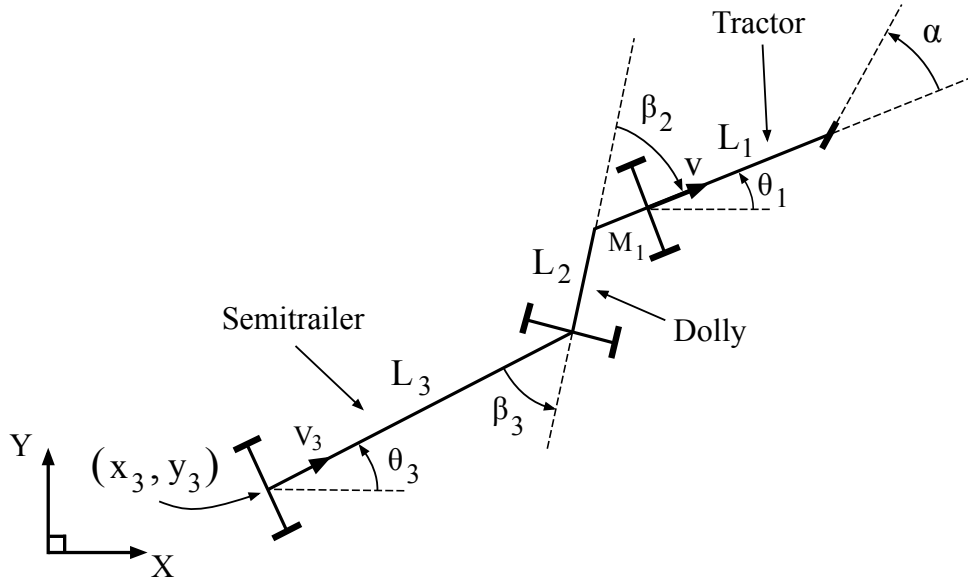


Figure 2: A schematic description of the geometric lengths, states and control inputs that are of relevance for modeling the G2T with a car-like tractor.

therefore without loss of generality further assumed that the velocity of the tractor is restricted to $v \in \{-1, 1\}$, where $v = 1$ denotes forward motion and $v = -1$ backward motion. The direction of motion is essential for the stability of the system (1), where the joint-angle kinematics are structurally unstable in backward motion ($v < 0$), where it risks to fold and enter a jack-knife state [3]. In forward motion ($v > 0$), these modes are stable but in case of positive off-axle hitching ($M_1 > 0$), some of the system's output channels poses non-minimum phase properties (see, e.g., [35] for an analysis).

2.1 Constraints

The car-like tractor is assumed to have physical bounds on its curvature u and curvature rate \dot{u} , which are modeled as box constraints

$$|u| \leq u_{\max}, \quad |\dot{u}| \leq \dot{u}_{\max}, \quad (3)$$

where the positive constants u_{\max} and \dot{u}_{\max} denote maximum curvature and curvature rate, respectively. In practice, advanced sensors mounted in the rear of the car-like tractor have been proposed as solutions to the joint-angle estimation problem [9, 27, 44]. Such sensors typically have a limited FOV which enforce non-convex restrictions on the set of joint angles that can be estimated with high accuracy. Additionally, constraints on the joint angles that prevent the vehicle from entering a jack-knife state should also be considered. The above mentioned re-

restrictions on β_2 and β_3 are assumed to be described by a union of $n \in \mathbb{Z}_+$ convex polytopes \mathbb{P}_i in the form

$$\mathbb{X} = \bigcup_{i=1}^n \mathbb{P}_i = \bigcup_{i=1}^n \left\{ (\beta_3, \beta_2) \in \mathbb{R}^2 \mid H_i (\beta_3 \quad \beta_2)^T \leq h_i \right\}, \quad (4)$$

where $H_i \in \mathbb{R}^{m_i \times 2}$, $h_i \in \mathbb{R}^{m_i}$ and $m_i \in \mathbb{Z}_+$ for $i = 1, \dots, n$. The set \mathbb{X} is assumed to be closed, compact and contain the origin $(\beta_2, \beta_3) = (0, 0)$ in its interior. For compactness, the constraint in (4) is represented as $(\beta_3, \beta_2) \in \mathbb{X}$. Note that if $n \geq 2$, the set in (4) is in general a non-convex set and if $n = 1$, it is a set of linear inequality constraints.

Even though the constraints in (3) and (4) have been considered by the motion planner while computing the motion plan, disturbances are always present during plan execution making it important to also consider them in the controller.

2.2 Path-following error model

Given a nominal trajectory $(x_r(\cdot), u_r(\cdot), v_{3r}(\cdot))$ satisfying the model of the G2T with a car-like tractor (1):

$$\dot{x}_r = v_{3r} f(x_r, u_r), \quad (5)$$

which is assumed to satisfy the constraints in (3) and (4). Except from satisfying the constraints, the objective of the path-following controller is to control the tractor's curvature u such that the motion plan obtained from the motion planner is followed with a small and bounded path-following error. Similar to [27], this is performed by first deriving a path-following error model that describes the vehicle in terms of deviation from a nominal path. Given the vehicle's current state $x(t)$, define $s(t)$ as the distance traveled by the position of the semitrailer's axle onto its projection to its nominal path $(x_{3r}(\cdot), y_{3r}(\cdot))$ up to time t . Since $\frac{dx_r}{dt} = \frac{dx_r}{ds} |v_{3r}|$, the nominal trajectory in (5) can instead be interpreted as a nominal path

$$\frac{dx_r}{ds} = \bar{v}_{3r} f(x_r, u_r), \quad (6)$$

where $\bar{v}_{3r} = \text{sign}(v_{3r}) \in \{-1, 1\}$ represents the nominal motion direction, i.e., $\bar{v}_{3r} = 1$ represents forward motion and $\bar{v}_{3r} = -1$ backward motion.

To exploit that a nominal path (6) is provided, the G2T with car-like tractor in (1) is first modeled in terms of deviation from this nominal path, as illustrated in Figure 3. Denote $\tilde{z}_3(t)$ as the signed lateral distance between the center of the semitrailer's axle $(x_3(t), y_3(t))$ and its projection to its nominal path in $(x_{3r}(\cdot), y_{3r}(\cdot))$. Define the orientation error of the semitrailer as $\tilde{\theta}_3(t) = \theta_3(t) - \theta_{3r}(s(t))$, and define joint-angle errors as $\tilde{\beta}_3(t) = \beta_3(t) - \beta_{3r}(s(t))$ and $\tilde{\beta}_2(t) =$

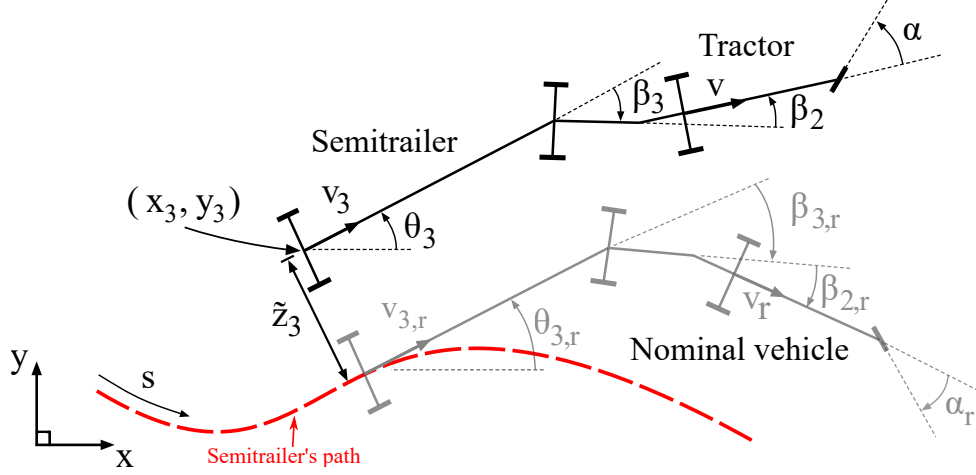


Figure 3: The G2T with a car-like tractor in the Frenet frame path coordinate system.

$\beta_2(t) - \beta_{2r}(s(t))$. Finally, define the controlled curvature deviation as $\tilde{u}(t) = u(t) - u_r(s(t))$. Using the Frenet-frame transformation together with the chain rule (see [27] for details), the G2T with a car-like tractor (1) can be modeled in terms of deviation from the nominal path (6) as

$$\dot{s} = v_3 \frac{\bar{v}_{3r} \cos \tilde{\theta}_3}{1 - \kappa_{3r} \tilde{z}_3}, \quad (7a)$$

$$\dot{\tilde{z}}_3 = v_3 \sin \tilde{\theta}_3, \quad (7b)$$

$$\dot{\tilde{\theta}}_3 = v_3 \left(\frac{\tan(\tilde{\beta}_3 + \beta_{3r})}{L_3} - \frac{\kappa_{3r} \cos \tilde{\theta}_3}{1 - \kappa_{3r} \tilde{z}_3} \right), \quad (7c)$$

$$\begin{aligned} \dot{\tilde{\beta}}_3 = v_3 & \left(\frac{\sin(\tilde{\beta}_2 + \beta_{2r}) - M_1 \cos(\tilde{\beta}_2 + \beta_{2r})(\tilde{u} + u_r)}{L_2 C_1(\tilde{\beta}_2 + \beta_{2r}, \tilde{\beta}_3 + \beta_{3r}, \tilde{u} + u_r)} - \frac{\tan(\tilde{\beta}_3 + \beta_{3r})}{L_3} \right. \\ & \left. - \frac{\cos \tilde{\theta}_3}{1 - \kappa_{3r} \tilde{z}_3} \left[\frac{\sin \beta_{2r} - M_1 \cos \beta_{2r} u_r}{L_2 C_1(\beta_{2r}, \beta_{3r}, u_r)} - \kappa_{3r} \right] \right), \end{aligned} \quad (7d)$$

$$\dot{\tilde{\beta}}_2 = v_3 \left(\left[\frac{\tilde{u} + u_r - \frac{\sin(\tilde{\beta}_2 + \beta_{2r})}{L_2} + \frac{M_1 \cos(\tilde{\beta}_2 + \beta_{2r})(\tilde{u} + u_r)}{L_2}}{C_1(\tilde{\beta}_2 + \beta_{2r}, \tilde{\beta}_3 + \beta_{3r}, \tilde{u} + u_r)} \right] - \frac{\cos \tilde{\theta}_3}{1 - \kappa_{3r} \tilde{z}_3} \left[\frac{u_r - \frac{\sin \beta_{2r}}{L_2} + \frac{M_1 \cos \beta_{2r} u_r}{L_2}}{C_1(\beta_{2r}, \beta_{3r}, u_r)} \right] \right), \quad (7e)$$

where

$$\kappa_{3r}(s) = \frac{d\theta_{3r}}{ds} = \frac{\tan \beta_{3r}(s)}{L_3}, \quad (8)$$

is the nominal curvature for the center of the semitrailer's axle. The transformation to the Frenet frame path-coordinate system is valid as long as \tilde{z}_3 and $\tilde{\theta}_3$ satisfy

$$\kappa_{3r}(s) \tilde{z}_3 < 1, \quad |\tilde{\theta}_3| < \pi/2. \quad (9)$$

The former constraint can be approximated as $|\tilde{z}_3| \leq \tilde{z}_3^{\max}$, where the constant $\tilde{z}_3^{\max} < 1/\kappa_{3r}^{\max}$, where κ_{3r}^{\max} is the maximum curvature of the nominal path in $(x_{3r}(\cdot), y_{3r}(\cdot))$. Note that \bar{v}_{3r} is included in (7a) to make $\dot{s} > 0$ as long as the constraints in (9) are satisfied, and the semitrailer's velocity v_3 and its nominal motion direction \bar{v}_{3r} have the same sign. Since it is required that $C_1(\beta_2, \beta_3, u) > 0$ and the relationship $v = v_3 C_1(\beta_2, \beta_3, u)$ holds, this is equivalent to that tractor's velocity v is selected such that $\text{sign}(v) = \bar{v}_{3r}$.

Define the path-following error state $\tilde{x} = [\tilde{z}_3 \ \tilde{\theta}_3 \ \tilde{\beta}_3 \ \tilde{\beta}_2]^T$, where its model is given by (7b)–(7e). It is easily verified that the origin $(\tilde{x}, \tilde{u}) = (0, 0)$ to this system is an equilibrium point for all $s(t)$. Moreover, since the velocity of the car-like tractor v is selected such that $\dot{s}(t) > 0$, it is possible to perform time-scaling [41] and eliminate the time-dependency presented in (7b)–(7e). Using the chain rule, it holds that $\frac{d\tilde{x}}{ds} = \frac{d\tilde{x}}{dt} \frac{1}{\dot{s}}$, and the spatial version of the path-following error model (7b)–(7e) becomes

$$\frac{d\tilde{z}_3}{ds} = \bar{v}_{3r}(1 - \kappa_{3r}\tilde{z}_3) \tan \tilde{\theta}_3, \quad (10a)$$

$$\frac{d\tilde{\theta}_3}{ds} = \bar{v}_{3r} \left([1 - \kappa_{3r}\tilde{z}_3] \frac{\tan(\tilde{\beta}_3 + \beta_{3r})}{L_3 \cos \tilde{\theta}_3} - \kappa_{3r} \right), \quad (10b)$$

$$\begin{aligned} \frac{d\tilde{\beta}_3}{ds} = \bar{v}_{3r} \left(\frac{1 - \kappa_{3r}\tilde{z}_3}{\cos \tilde{\theta}_3} \left[\frac{\sin(\tilde{\beta}_2 + \beta_{2r}) - M_1 \cos(\tilde{\beta}_2 + \beta_{2r})(\tilde{u} + u_r)}{L_2 C_1(\beta_{2r} + \tilde{\beta}_2, \beta_{3r} + \tilde{\beta}_3, u_r + \tilde{u})} \right. \right. \\ \left. \left. - \frac{\tan(\tilde{\beta}_3 + \beta_{3r})}{L_3} \right] - \left[\frac{\sin \beta_{2r} - M_1 \cos \beta_{2r} u_r}{L_2 C_1(\beta_{2r}, \beta_{3r}, u_r)} - \kappa_{3r} \right] \right), \end{aligned} \quad (10c)$$

$$\begin{aligned} \frac{d\tilde{\beta}_2}{ds} = \bar{v}_{3r} \left(\frac{1 - \kappa_{3r}\tilde{z}_3}{\cos \tilde{\theta}_3} \left[\frac{\tilde{u} + u_r + \frac{M_1}{L_2} \cos(\tilde{\beta}_2 + \beta_{2r})(\tilde{u} + u_r)}{C_1(\beta_{2r} + \tilde{\beta}_2, \beta_{3r} + \tilde{\beta}_3, u_r + \tilde{u})} \right. \right. \\ \left. \left. - \frac{\sin(\tilde{\beta}_2 + \beta_{2r})}{L_2 C_1(\beta_{2r} + \tilde{\beta}_2, \beta_{3r} + \tilde{\beta}_3, u_r + \tilde{u})} \right] - \left[\frac{u_r - \frac{\sin \beta_{2r}}{L_2} + \frac{M_1}{L_2} \cos \beta_{2r} u_r}{C_1(\beta_{2r}, \beta_{3r}, u_r)} \right] \right), \end{aligned} \quad (10d)$$

which can compactly be represented as $\frac{d\tilde{x}}{ds} = \tilde{f}(s, \tilde{x}, \tilde{u})$, where the origin $(\tilde{x}, \tilde{u}) = (0, 0)$ is an equilibrium point for all s .

3 Model predictive path-following controller

The task of the MPC controller is to control the tractor's curvature u such that the path-following error is minimized while the vehicle's constraints (3)–(4) are satisfied for all time instances. Since the vehicle's joint angles are restricted to a union of convex polytopes (4), binary decision variables are in general needed to incorporate these constraints within the MPC controller.

Therefore, due to the combination of binary and continuous variables, the resulting MPC problem will be in the form of a mixed-integer programming (MIP) problem. To obtain an MIP problem that has the potential of being solved at a sufficiently high rate, each subproblem when the binary variables are fixed should be simple to solve. As a consequence, the aim is to derive an MPC formulation that can be converted into the form of an MIQP problem, where efficient state-of-the-art commercial MIQP solvers exist, such as Gurobi [17] and CPLEX [20].

First, the nonlinear path-following error model (10) is linearized around the origin $(\tilde{x}, \tilde{u}) = (0, 0)$:

$$\frac{d\tilde{x}}{ds} = A(s)\tilde{x} + B(s)\tilde{u}, \quad (11)$$

where the distance-varying matrices $A(s)$ and $B(s)$ are presented in Appendix A. With the sampling distance Δ_s , Euler-forward discretization yields a discrete approximation of (11) in the form

$$\tilde{x}_{k+1} = F_k\tilde{x}_k + G_k\tilde{u}_k, \quad (12)$$

where

$$F_k = I + \Delta_s A_k, \quad G_k = \Delta_s B_k. \quad (13)$$

Since the tractor's curvature is $u_k = \tilde{u}_k + u_{r,k}$, the deviation in the curvature is bounded as

$$-u_{\max} \leq \tilde{u}_k + u_{r,k} \leq u_{\max}. \quad (14)$$

Moreover, since $\dot{s} > 0$ the constraint on the tractor's curvature rate $|\dot{u}| \leq \dot{u}_{\max}$ can be described in s using the chain rule as

$$\left| \frac{du}{ds} \right| \leq \frac{\dot{u}_{\max}}{\dot{s}} = \frac{1 - \kappa_{3r}\tilde{z}_3}{|v|C_1(\beta_2, \beta_3, u)\cos\tilde{\theta}_3} \dot{u}_{\max}, \quad (15)$$

since $v_3 = vC_1(\beta_2, \beta_3, u)$. Locally around the nominal path $(\tilde{x}, \tilde{u}) = (0, 0)$, it holds that $\cos\tilde{\theta}_3 \approx 1$ and $\kappa_{3r}\tilde{z}_3 \approx 0$. Thus, to avoid coupling between \tilde{x} and \tilde{u} , the constraint in (15) is approximated as

$$\left| \frac{du}{ds} \right| \leq \frac{\dot{u}_{\max}}{|v|C_1(\beta_{2r}(s), \beta_{3r}(s), u_r(s))} \triangleq c_{\max}(s). \quad (16)$$

By discretizing (16) using Euler forward, the rate limit on the controlled curvature deviation can be described by the following slew-rate constraint

$$-c_{\max,k}\Delta_s \leq \tilde{u}_k - \tilde{u}_{k-1} - \bar{u}_{r,k} \leq c_{\max,k}\Delta_s, \quad (17)$$

where $\bar{u}_{r,k} = u_{r,k} - u_{r,k-1}$. Denote the linear inequality constraints in (14) and (17) as $\tilde{u}_k \in \tilde{\mathcal{U}}_k$. What remains is to describe the non-convex joint-angle constraint (4) as a function of \tilde{x} and to model it in an MIQP representable form. Since the joint angles are $\beta_{j,k} = \beta_{jr,k} + \tilde{\beta}_{j,k}$, $j = 2, 3$, each convex polytope \mathbb{P}_i , $i = 1, \dots, n$ that is used to model the constraint on the joint angles (4) can be written as

$$H_i \begin{bmatrix} \tilde{\beta}_{3,k} \\ \tilde{\beta}_{2,k} \end{bmatrix} \leq h_i - H_i \begin{bmatrix} \beta_{3r,k} \\ \beta_{2r,k} \end{bmatrix} = \bar{h}_{i,k}, \quad (18)$$

which is denoted as $(\tilde{\beta}_{3,k}, \tilde{\beta}_{2,k}) \in \tilde{\mathbb{P}}_{i,k}$. Now, at each sample k along the future prediction horizon, a binary decision variable is introduced $\delta_{i,k} = \{0, 1\}$ to indicate if $(\tilde{\beta}_{3,k}, \tilde{\beta}_{2,k}) \in \tilde{\mathbb{P}}_{i,k}$. Using logical implications, this can be enforced using hybrid logic on the constraint on the joint angles with

$$\delta_{i,k} \rightarrow (\tilde{\beta}_{3,k}, \tilde{\beta}_{2,k}) \in \tilde{\mathbb{P}}_{i,k}, \quad i = 1, \dots, n. \quad (19)$$

Define $\bar{\delta}_k = [\delta_{1,k} \ \delta_{2,k} \ \dots \ \delta_{n,k}]^T \in \{0, 1\}^n$ as a binary vector and by adding the constraint $\sum_{i=1}^n \delta_{i,k} = 1$, the logical model ensures that the joint angles are in at least one of the convex polytopes at sample k . The logical implications are easily converted to linear inequality constraints using big-M modeling strategies, but the details are omitted, as the employed modeling tool YALMIP [28] will do this step automatically given the logical model.

Given the current path-following error state $\tilde{x}(s(t))$, the MPC problem with prediction horizon N is defined as

$$\underset{\tilde{\mathbf{x}}, \tilde{\mathbf{u}}, \boldsymbol{\delta}}{\text{minimize}} \quad V_N(\tilde{\mathbf{x}}, \tilde{\mathbf{u}}) = V_f(\tilde{x}_N) + \sum_{k=0}^{N-1} l(\tilde{x}_k, \tilde{u}_k) \quad (20a)$$

$$\text{subject to} \quad \tilde{x}_{k+1} = F_k \tilde{x}_k + G_k \tilde{u}_k, \quad k = 0, 1, \dots, N-1, \quad (20b)$$

$$\delta_{i,k} \rightarrow (\tilde{\beta}_{3,k}, \tilde{\beta}_{2,k}) \in \tilde{\mathbb{P}}_{i,k}, \quad i = 1, \dots, n, \quad k = 0, 1, \dots, N-1, \quad (20c)$$

$$\sum_{i=1}^n \delta_{i,k} = 1, \quad \tilde{u}_k \in \tilde{\mathcal{U}}_k, \quad k = 0, 1, \dots, N-1, \quad (20d)$$

$$|\tilde{z}_{3,k}| \leq \tilde{z}_3^{\max}, \quad |\tilde{\theta}_{3,k}| \leq \tilde{\theta}_3^{\max}, \quad k = 0, 1, \dots, N-1, \quad (20e)$$

$$\tilde{x}_0 = \tilde{x}(s(t)) \text{ given}, \quad (20f)$$

where $\tilde{\mathbf{x}}^T = [\tilde{x}_0^T \ \tilde{x}_1^T \ \dots \ \tilde{x}_N^T]$ is the predicted path-following error state-vector sequence, $\tilde{\mathbf{u}} = [\tilde{u}_0 \ \tilde{u}_1 \ \dots \ \tilde{u}_{N-1}]^T$ is the curvature-deviation sequence and $\boldsymbol{\delta}^T = [\bar{\delta}_0^T \ \bar{\delta}_1^T \ \dots \ \bar{\delta}_{N-1}^T]$ is the binary-vector sequence. In (20e), the constants \tilde{z}_3^{\max} and $\tilde{\theta}_3^{\max} < \pi/2$ are the semitrailer's maximum lateral and orientation error, respectively. The stage-cost is chosen as $l(\tilde{x}_k, \tilde{u}_k) = \tilde{x}_k^T Q \tilde{x}_k + \tilde{u}_k^2$ and the terminal-cost $V_f(\tilde{x}_N) = \tilde{x}_N^T P_N \tilde{x}_N$, where $Q \succeq 0$ and $P_N \succ 0$ are design matrices of appropriate

dimensions. Since the cost function V_N is quadratic and there are only linear equality and inequality constraints for a fixed binary-vector sequence, the MPC problem (20) can be converted into an MIQP problem.

Remark 1. *If the constraint on the joint angles (4) is modeled as a single polytope ($n = 1$), binary variables are not needed and the MPC problem (20) simplifies to a QP problem.*

At each sampling instance, the MPC problem (20) is solved to obtain the optimal open-loop controlled curvature deviation sequence $\tilde{\mathbf{u}}^*$. As in standard receding horizon control, only the first control input \tilde{u}_0^* is used

$$u(t) = u_r(s(t)) + \tilde{u}_0^*, \quad (21)$$

and the optimizing problem (20) is repeatedly solved at each sampling instance using new state information. Note that the MPC controller only computes the feedback part of the control signal, as the optimal feed forward $u_r(s(t))$ already is provided by the motion planner.

4 Estimation-aware controller design

In this section, the control design of the proposed model predictive path-following controller (20) is presented. It is tailored for the case when a rear-view LIDAR with a limited FOV is used as part of the estimation solution [27]. However, note that similar techniques can also be used if a rear-view camera or RADAR is used as sensor.

4.1 Design of cost function

Since a nominal path that satisfies the vehicle model (6) is provided, it is possible to calculate the nominal paths for the position and orientation of the dolly as well as the car-like tractor using the nominal state path $x_r(\cdot)$ together with holonomic relationships [1]. To reduce the risk of colliding with surrounding obstacles, it is desired that the MPC controller is tuned such that the transient response of all path-following errors are prioritized. Denote \tilde{z}_1 and \tilde{z}_2 as the signed lateral distances of the axle of the dolly and the car-like tractor onto their nominal paths, see Figure 4. Moreover, define their corresponding orientation errors as $\tilde{\theta}_1 = \theta_1 - \theta_{1r}$ and $\tilde{\theta}_2 = \theta_2 - \theta_{2r}$, respectively. In general, it is not possible to derive a closed-form expression to describe these additional path-following error states as a function of the modeled path-following error states \tilde{x} (see [2] for details). However, for the special case of a straight nominal path, closed-form expressions exist and the signed lateral errors \tilde{z}_2 and \tilde{z}_1 can be described as

$$\tilde{z}_2 = \tilde{z}_3 + L_3 \sin \tilde{\theta}_3, \quad (22a)$$

$$\tilde{z}_1 = \tilde{z}_2 + L_2 \sin(\tilde{\theta}_3 + \tilde{\beta}_3) + M_1 \sin(\tilde{\theta}_3 + \tilde{\beta}_3 + \tilde{\beta}_2), \quad (22b)$$

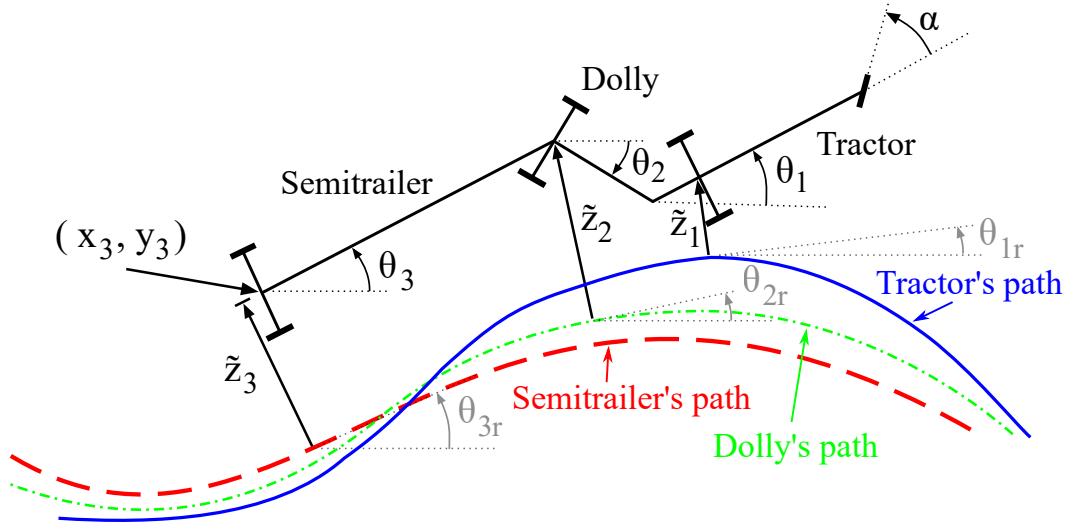


Figure 4: Illustration of the additional path-following error states that are used in the design of the MPC controller.

and their corresponding orientation errors $\tilde{\theta}_2$ and $\tilde{\theta}_1$ as

$$\tilde{\theta}_2 = \tilde{\theta}_3 + \tilde{\beta}_3, \quad (23a)$$

$$\tilde{\theta}_1 = \tilde{\theta}_3 + \tilde{\beta}_3 + \tilde{\beta}_2. \quad (23b)$$

Using these approximate relationships also for arbitrary nominal paths the control-measure vector is defined as

$$z = [\tilde{z}_1 \quad \tilde{\theta}_1 \quad \tilde{z}_2 \quad \tilde{\theta}_2 \quad \tilde{\beta}_2 \quad \tilde{z}_3 \quad \tilde{\theta}_3 \quad \tilde{\beta}_3]^T \triangleq h(\tilde{x}). \quad (24)$$

The function $h(\tilde{x})$ is nonlinear and its Jacobian linearization around the origin yields $z = \frac{\partial h(0)}{\partial \tilde{x}} \tilde{x} \triangleq M\tilde{x}$, where

$$M = \begin{bmatrix} 1 & L_3 + L_2 + M_1 & L_2 + M_1 & M_1 \\ 0 & 1 & 1 & 1 \\ 1 & L_3 & 0 & 0 \\ 0 & 1 & 1 & 0 \\ 0 & 0 & 0 & 1 \\ 1 & 0 & 0 & 0 \\ 0 & 1 & 0 & 0 \\ 0 & 0 & 1 & 0 \end{bmatrix}. \quad (25)$$

By selecting the weight matrix for the quadratic stage-cost as $Q = M^T \bar{Q} M$, where $\bar{Q} \succeq 0$ is a diagonal matrix, each diagonal element in \bar{Q} corresponds to penalizing a specific control objective in z .

After the weight matrix Q has been selected, the weight matrix $P_N \succ 0$ for the terminal cost is selected as the solution to the discrete-time algebraic Riccati equation (DARE):

$$F^T P_N F - P_N - F^T P_N G K + Q = 0, \quad (26)$$

where $K = (1 + G^T P_N G)^{-1} G^T P_N F$ is the LQ feedback gain, and the matrices $F = I + \Delta_s A$ and $G = \Delta_s B$ are the discrete-time system matrices (13) for the linearized path-following error model (12) around a straight nominal path. In this case, the matrices A and B are given by

$$A = \bar{v}_{3r} \begin{bmatrix} 0 & 1 & 0 & 0 \\ 0 & 0 & \frac{1}{L_3} & 0 \\ 0 & 0 & -\frac{1}{L_3} & \frac{1}{L_2} \\ 0 & 0 & 0 & -\frac{1}{L_2} \end{bmatrix}, \quad B = \bar{v}_{3r} \begin{bmatrix} 0 \\ 0 \\ \frac{-M_1}{L_2} \\ \frac{L_2 + M_1}{L_2} \end{bmatrix}, \quad (27)$$

where $v_{3r} \in \{-1, 1\}$ specifies the nominal motion direction. Thus, since the system's stability properties vary depending on the direction of motion, different terminal costs are used during backward and forward motion tasks [27].

4.2 Modeling of the constraint on the joint angles

The constraint on the joint angles (4) is intended to be selected such that the system avoids jackknifing, but also to restrict the joint angles to remain in the region where the used state-estimation solution is able to compute reliable and accurate state estimates of the trailer pose and the joint angles.

Since the tractor's curvature is limited by (14) and (17), it is not possible to globally stabilize the path-following error system (10) since for sufficiently large joint angles, jackknifing is impossible to prevent by only driving backwards [3]. This limit is possible to calculate analytically for the single-trailer case, but approximate methods are most often utilized when more than one trailer is present [3]. Given a straight nominal path, the vehicle parameters presented in Table 1, the MPC controller in (20) with no joint-angle constraints and the design parameters in Table 2. This system is simulated from different initial joint angles in backward motion with $v = -1$ m/s and is checked for convergence onto the straight nominal path. Using this technique, it is possible to numerically evaluate from which joint angles the closed-loop system is able to recover from and which will lead to jackknifing. The simulated stability region for the system is illustrated by the blue and green dots in Figure 5.

The sensor placement used in [27] is illustrated in Figure 6 together with a definition of relevant physical quantities that are also explained in Table 1. As long as the entire front of the semitrailer's body is visible from the LIDAR's point cloud, the LIDAR-based estimation technique presented in [27] computes accurate estimates of the joint angles as well as the remaining

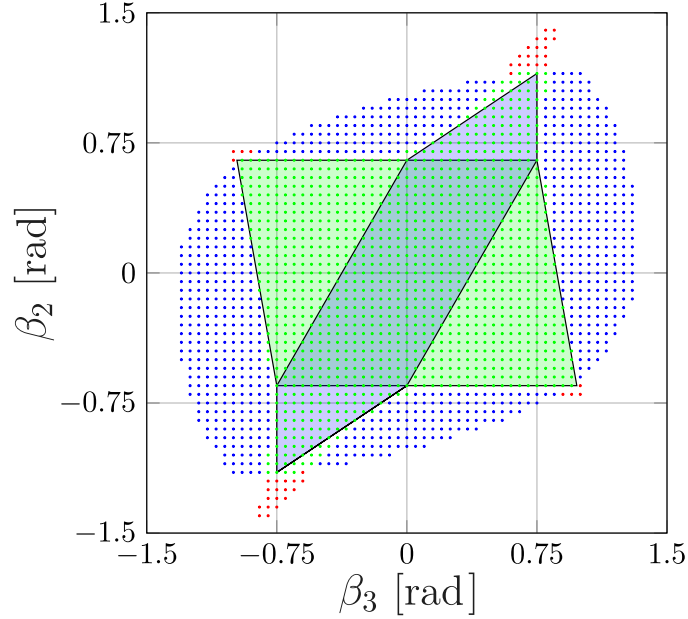


Figure 5: The simulated stability region for different joint angles (blue and green dots) around a straight nominal path and the region where the LIDAR-based estimation solution can compute estimates of the joint angles (red and green dots). The union of the blue and green polytopes is used to model the constraint for the joint angles (4).

states of the semitrailer. Geometrically, this is equivalent to the following two conditions. First, the two corners, p_1 and p_2 , of the semitrailer's front are inside the LIDAR's FOV. Second, the placement of the LIDAR is inside the half-space ahead of the semitrailer's front (green area in Figure 6).

To model these conditions, a local coordinate system is introduced that is aligned with the tractor's orientation and has its origin at the tractor's off-axle hitch connection. Using basic trigonometry, the positions for the two corners of the semitrailer's front $p_1 = (x_{p_1}, y_{p_1})$ and $p_2 = (x_{p_2}, y_{p_2})$, can be expressed as a function of β_2 and β_3 , and the vehicle parameters L_2 , L_a and b . Define angle of the sensor's horizontal scan field as ϕ , then the following inequality constraints have to be satisfied for the two features¹, p_1 and p_2 , to lie within the LIDAR's FOV:

$$\cos\left(\frac{\phi}{2}\right)y_{p_i} + \sin\left(\frac{\phi}{2}\right)x_{p_i} \leq 0, \quad (28a)$$

$$\cos\left(\frac{\phi}{2}\right)y_{p_i} - \sin\left(\frac{\phi}{2}\right)x_{p_i} \geq 0, \quad i = 1, 2. \quad (28b)$$

¹Note that it is straightforward to use the proposed design strategy for other types of advanced sensors (e.g., camera or RADAR) and if other features on the semitrailer's body are important to keep in the sensor's FOV.

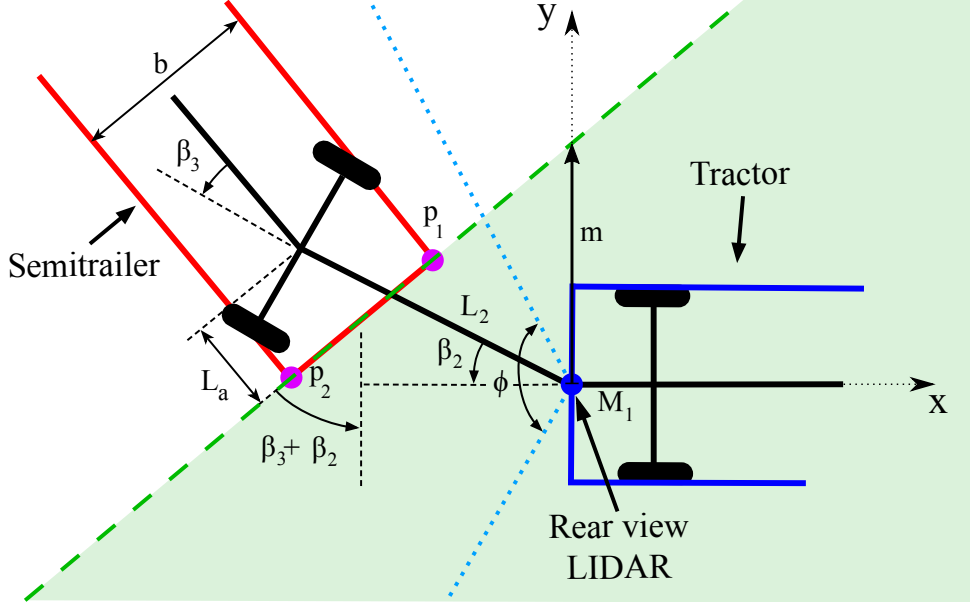


Figure 6: Illustration of the placement of the rear-view LIDAR sensor, its FOV (blue dotted lines) and relevant physical quantities.

Furthermore, the border of the half-space that is ahead of the semitrailer's front (green dashed line in Figure 6) can be expressed as

$$\sin(\beta_2 + \beta_3)y - \cos(\beta_2 + \beta_3)x = \bar{m}, \quad (29)$$

where $\bar{m} = L_2 \cos \beta_3 - L_a$. When $\beta_2 + \beta_3 \neq 0$, the line in (29) intersects the y-axis in the tractor's local coordinate system at $m = \bar{m} / \sin(\beta_2 + \beta_3)$. Hence, for the placement of the rear-view LIDAR sensor to strictly lie inside the half-space ahead of the semitrailer's front, one of the following three conditions has to be satisfied

$$\beta_2 + \beta_3 > 0 \text{ and } m \leq \varepsilon, \quad (30a)$$

$$\beta_2 + \beta_3 < 0 \text{ and } m \geq -\varepsilon, \quad (30b)$$

$$\beta_2 + \beta_3 = 0 \text{ and } L_a - L_2 \cos \beta_2 \leq -\varepsilon, \quad (30c)$$

where $\varepsilon > 0$ is a constant that is used to enforce a certain robustness margin. Given the vehicle parameters in Table 1 and the robustness margin $\varepsilon = 1$ m, the joint angles that satisfy the above mentioned constraints are illustrated by the green and red dots in Figure 5. As can be seen, the numerically computed stability region for the closed-loop system in backward motion (blue and green dots in Figure 5) is almost completely covering the region where accurate state estimates can be computed.

The constraint on the joint angles (4) is now modeled as an inner approximation of the intersection of these two sets which is represented by the green dots in Figure 5. Based on

the method used to represent this inner approximation, two alternative MPC controllers are proposed:

- The union of two convex polytopes (The blue and green polytopes in Figure 5) is used as inner approximation. Two binary decision variables ($n = 2$) are therefore introduced in the MIQP-MPC controller (20).
- A single convex polytope (e.g. green polytope in Figure 5) is used to obtain an inner approximation. In this case, no binary decision variables are needed in the QP-MPC controller (20).

The computational complexity of these two MPC controllers differs substantially because the MIQP-MPC controller requires that an MIQP problem is solved at each sampling instance, whereas the QP-MPC controller only needs to solve a QP problem. However, since the QP-MPC controller is restricted to use a single convex polytope to model the constraint on the joint angles, its performance may become noticeably suboptimal unless the polytope is carefully selected. To analyze the impact of this choice, different convex polytopes will be evaluated in the result section. Finally, since the vehicle model used in the MPC controllers only is an approximation, the hard constraints on the joint angles as well as the constraints on the semitrailer’s lateral and orientation errors are replaced with soft constraints using standard techniques [13, 16, 29].

5 Results

The performance of the proposed estimation-aware MPC approach is first evaluated in a simulation study and then in field experiments using the full-scale tractor-trailer vehicle shown in Figure 1. Due to the extensive work-load required to interface an MIQP solver on the test vehicle, only the QP-MPC controller is experimentally validated in the field experiments. The

Table 1: The vehicle parameters for the full-scale G2T with a car-like tractor.

Vehicle parameter	Value
The tractor’s wheelbase L_1	4.62 m
Maximum curvature u_{\max}	0.18 m^{-1}
Maximum curvature rate \dot{u}_{\max}	$0.13 \text{ m}^{-1}\text{s}^{-1}$
Length of the off-hitch M_1	1.66 m
Length of the dolly L_2	3.87 m
Length of the semitrailer L_3	8.00 m
Length of the semitrailer’s overhang L_a	1.73 m
Width of the semitrailer’s front b	2.45 m
Angle of the horizontal scan field for the LIDAR ϕ	$140 \times \pi/180 \text{ rad}$

Table 2: Design parameters for the MPC controllers.

Design parameter	Value
Prediction horizon N_{QP}	40
Prediction horizon N_{MIQP}	30
Weight matrix \bar{Q}	$1/35 \times \text{diag}([0.5, 1, 0.5, 1, 4, 0.5, 1, 4])$
Sampling distance Δ_s	0.2 m
Controller frequency f_s	10 Hz

implementation details for the simulations study and the field experiments are thoroughly explained in Section 5.1 and Section 5.3, respectively.

5.1 Simulation setup

The performance of the MIQP-MPC controller and the QP-MPC controller are evaluated in a simulation study of backward and forward tracking a straight and a figure-eight nominal path. To enable rapid prototyping, the MPC controllers have been implemented in Matlab using YALMIP [28], where the state-of-the-art commercial MIQP solver Gurobi 8.1.1 [17] is used to solve (20) at each sampling instance for both MPC controllers. All simulations have been performed on a standard laptop computer with an Intel Core i7-4600U@2.1GHz CPU. The design parameters for the MPC controllers are listed in Table 2 and the vehicle parameters in Table 1. The vehicle parameters are selected to coincide with the full-scale test vehicle shown in Figure 1. As previously mentioned, since binary decision variables are not needed in the QP-MPC formulation it can be represented as a QP problem. This enables the use of a longer prediction horizon $N_{QP} = 40$ for the QP-MPC controller compared to a prediction horizon $N_{MIQP} = 30$ for the MIQP-MPC controller. Moreover, default settings are used in Gurobi with the exceptions that it is specified to perform warm starts and for MIQP-MPC to terminate once a solution with a relative suboptimality gap $\delta = 0.02$ is found.

The performance of the proposed MPC controllers are benchmarked with the LQ controller presented in [27]. The weight matrix Q is tuned equivalently for all controllers and the LQ feedback gains K_{fwd} and K_{rev} are computed offline by solving the DARE in (26) in Matlab with $v_{3r} = \pm 1$. It would be natural to compare the proposed approach with other path-following approaches [3,8,34,37,40]. However, since these approaches are not designed to follow nominal paths with full state and control-input information, a comparison is not included as the results would become misleading.

5.2 Simulation results

The first set of simulations involve backward tracking of a straight nominal path aligned with the x -axis ($y_{3r} = 0$), where the longitudinal velocity of the tractor is selected as $v = -1$ m/s. In

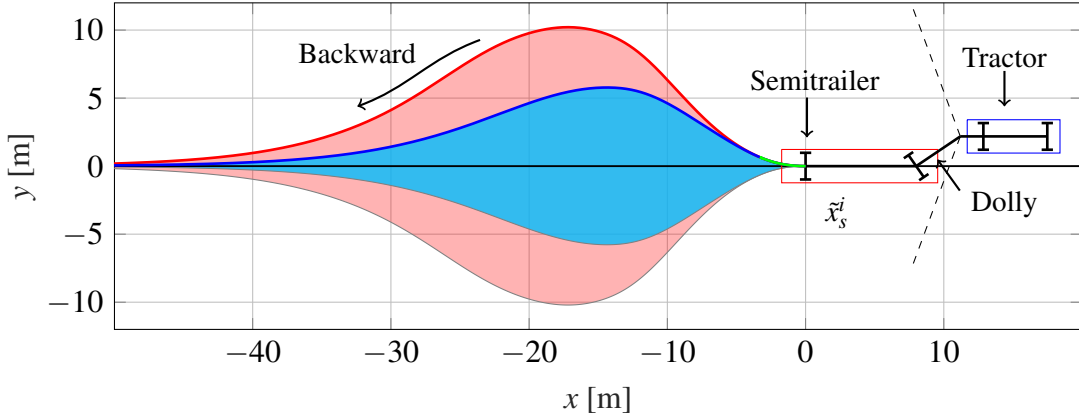
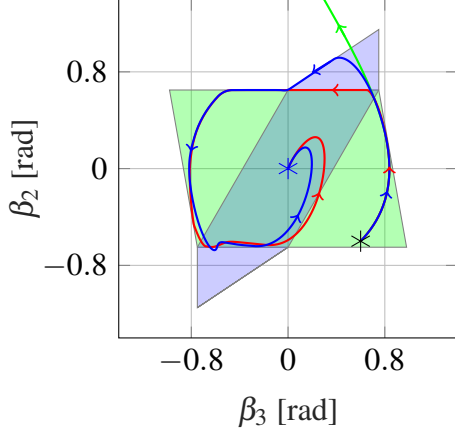


Figure 7: Envelopes of the trajectories for the axle of the semitrailer $(x_3(\cdot), y_3(\cdot))$ during backward tracking of a straight nominal path (black line), using MIQP-MPC (blue set) and QP-MPC (red set). For the high-lighted initial state \tilde{x}_s^i , the LQ controller leads to jackknifing (see Figure 8a.).

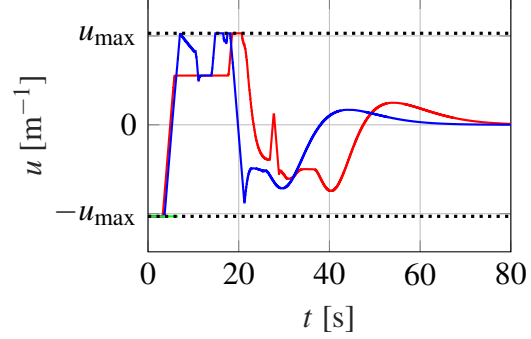
this case, the nominal $\beta_{3r} = \beta_{2r} = u_r = 0$ and therefore $\tilde{\beta}_3 = \beta_3$, $\tilde{\beta}_2 = \beta_2$ and $\tilde{u} = u$. In the simulations, the initial path-following error state $\tilde{x}(0)$ is perturbed to compare how the different controllers handle disturbance rejection while satisfying the constraint on the joint angles. The initial state is $\tilde{x}(0) = [0 \ 0 \ \beta_3^i \ \beta_2^i]^T$, where the initial joint-angle errors $\tilde{\beta}_3^i$ and $\tilde{\beta}_2^i$ are perturbed to various degrees. In this set of simulations, the green polytope shown in Figure 5 is used as the joint-angle constraint in the QP-MPC controller.

The results from the simulations are presented in Figure 7–8. The envelopes of the trajectories for the position of the semitrailer $(x_3(\cdot), y_3(\cdot))$ using MIQP-MPC and QP-MPC from initial joint-angle errors $\tilde{\beta}_3^i, \tilde{\beta}_2^i \in [-0.6, 0.6]$ rad are presented in Figure 7². The results show that the maximum transient in the lateral error of the semitrailer using the QP-MPC is 10.1 m in comparison to 5.7 m using the MIQP-MPC. The maximum convergence time to the straight nominal path is also longer using the QP-MPC compared to the MIQP-MPC. The reason why the MIQP-MPC outperforms the QP-MPC is because the MIQP-MPC exploits its larger joint-angle region (blue and green polytope in Figure 8a) in comparison to the QP-MPC controller’s more restrictive region (green polytope in Figure 8a). This can be observed in Figure 8a where the trajectories for the joint angles are provided from initial state \tilde{x}_s^i with initial joint-angle errors $(\tilde{\beta}_3^i, \tilde{\beta}_2^i) = (0.6, -0.6)$ rad. The results show that MIQP-MPC improves the convergence time and transient response by steering the vehicle such that the joint angles purely enters into the blue polytope for a small portion of the maneuver. This additional feasible joint-angle region is also used by the MIQP-MPC controller to reduce the maximum transient error in the semi-

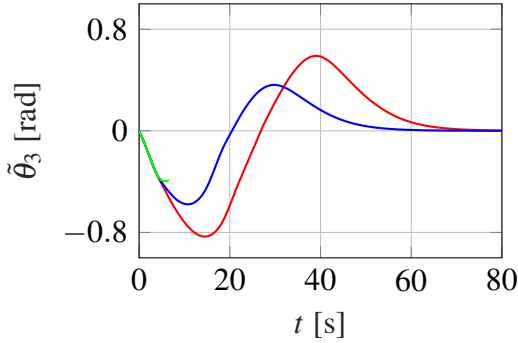
²The envelope for $(x_3(\cdot), y_3(\cdot))$ using the LQ controller is not presented in Figure 7 because the vehicle enters a jack-knife state for some $\tilde{\beta}_3^i, \tilde{\beta}_2^i \in [-0.6, 0.6]$ rad, e.g., from initial state \tilde{x}_s^i with $(\beta_3^i, \beta_2^i) = (0.6, -0.6)$ rad.



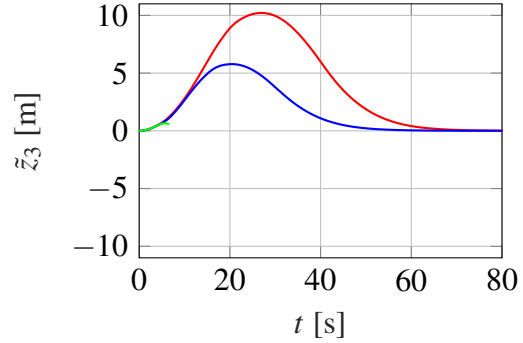
(a) The trajectories for the joint angles from initial state \tilde{x}_s^i in Figure 7. Initial (desired) state denoted by a black (blue) star.



(b) The car-like tractor's curvatures from \tilde{x}_s^i .



(c) The orientation errors from initial state \tilde{x}_s^i .



(d) The lateral errors from initial state \tilde{x}_s^i .

Figure 8: Simulation results from path following of a straight nominal path ($y_{3r} = 0$) in backward motion from perturbed initial joint-angle errors $\tilde{\beta}_3^i, \tilde{\beta}_2^i \in [-0.6, 0.6]$ rad, using MIQP-MPC (blue lines), QP-MPC (red lines) and LQ (green lines). High-lighted initial state \tilde{x}_s^i in Figure 7 is from $(\tilde{\beta}_3^i, \tilde{\beta}_2^i) = (0.6, -0.6)$ rad.

trailer's orientation error from initial state \tilde{x}_s^i (see Figure 8c) which is 0.57 rad in comparison to 0.81 rad for the QP-MPC controller. Moreover, the LQ controller is not able to stabilize the vehicle from \tilde{x}_s^i . This is because the LQ controller saturates the tractor's curvature (green line in Figure 8b) and since the system is open-loop unstable jackknifing occurs almost instantly (green line in Figure 8a).

The second set of simulations involve path following of a figure-eight nominal path in $(x_{3r}(\cdot), y_{3r}(\cdot))$ in both forward ($v = 1$ m/s) and backward motion ($v = -1$ m/s). The figure-eight nominal path has been computed following the steps presented in [27], which can be executed in both forward and backward motion because the system is symmetric [27]. Based on the results from the tracking of the straight nominal path, the convex polytope representing

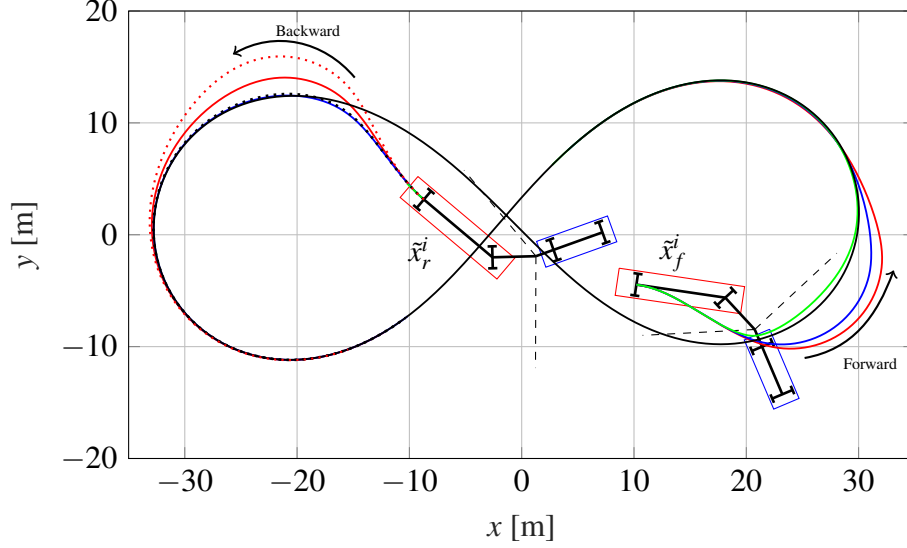
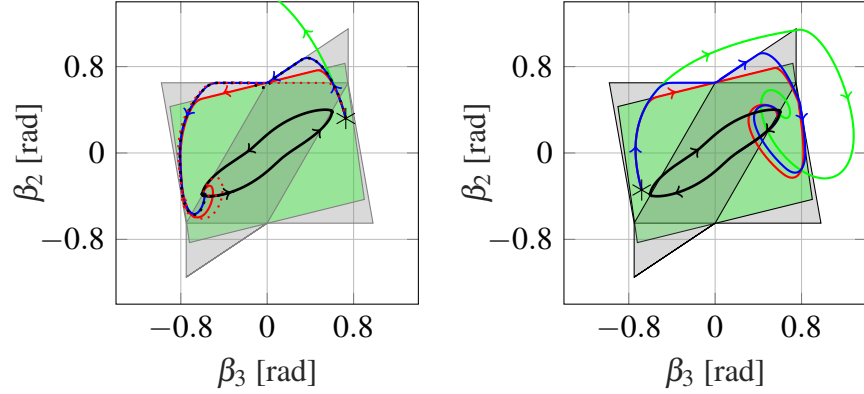


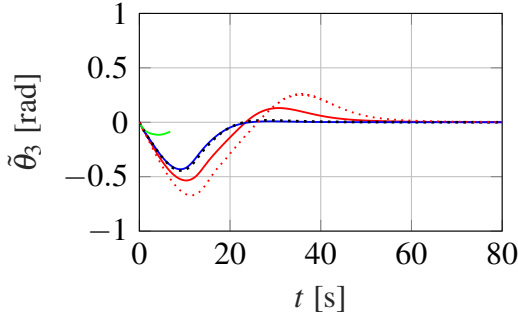
Figure 9: Simulation results from path following a figure-eight nominal path in $(x_{3r}(\cdot), y_{3r}(\cdot))$ (black line) using MIQP-MPC (blue lines), QP-MPC (red lines) and LQ (green lines) from initial state \tilde{x}_r^i in backward motion and from \tilde{x}_f^i in forward motion. From \tilde{x}_r^i , the LQ controller leads to jackknifing (see Figure 10a). The red dotted and black dotted lines are the trajectories from \tilde{x}_r^i using QP-MPC tuned as in the first set of simulations and using MIQP-MPC with termination criterion $\delta = 0.2$, respectively.

the joint-angle constraint in the QP-MPC controller is adjusted. The new constraint is illustrated by the green polytope in Figure 10a–10b. That is, the convex polytope has been rotated to increase the allowed joint-angle region where the joint angles have equal sign. Also in this set of simulations, the initial state $\tilde{x}(0)$ is perturbed to compare the performance of the controllers. The initial state is chosen as $\tilde{x}_r^i = [-4 \text{ m } 0 \text{ rad } 0.9 \text{ rad } 0.3 \text{ rad}]^T$ for the backward simulations and $\tilde{x}_f^i = [3 \text{ m } 0.4 \text{ rad } -1 \text{ rad } -0.7 \text{ rad}]^T$ for the forward simulations.

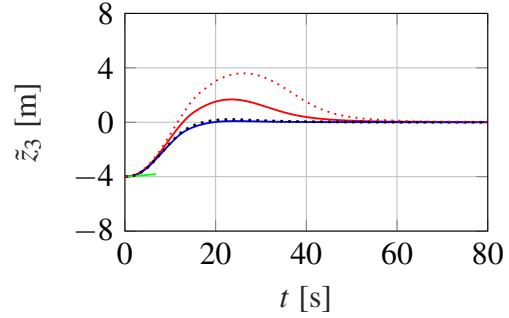
The simulation results are presented in Figure 9–10. For the backward simulations from \tilde{x}_r^i , the LQ controller is not able to stabilize the system and jackknifing occurs already after 5 seconds (see Figure 10a). As previously mentioned, this is because the LQ controller saturates the tractor’s curvature as it is not aware of its constraints (see Figure 10e). The QP-MPC controller converges to the figure-eight nominal path but with overshoots in both lateral error \tilde{z}_3 and orientation error $\tilde{\theta}_3$ of the semitrailer (red solid lines in Figure 10d–10c). However, by using the rotated polytope as constraint on the joint angles, the overshoots are decreased in comparison to the tuning used for QP-MPC in the first set of simulations (red-dotted lines in Figure 10). The MIQP-MPC controller is able to smoothly converge to the nominal path with no overshoot in \tilde{z}_3 nor in $\tilde{\theta}_3$ (blue lines in Figure 10d–10c). This performance enhancement is because the MIQP-MPC controller exploits its larger feasibility region in the joint angles. This can be seen in Figure 10a where the joint-angle trajectories $(\beta_2(\cdot), \beta_3(\cdot))$ are presented



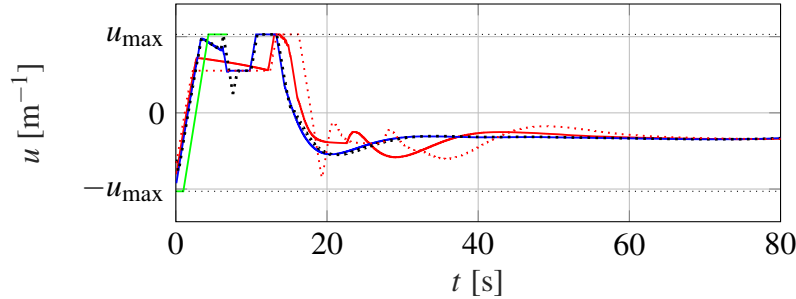
(a) The joint-angle trajectories from initial state \tilde{x}_r^i in Figure 9. The black line is the nominal path in $(\beta_{3r}(\cdot), \beta_{2r}(\cdot))$. (b) The joint-angle trajectories from initial state \tilde{x}_f^i in Figure 9. The black line is the nominal path in $(\beta_{3r}(\cdot), \beta_{2r}(\cdot))$.



(c) The orientation errors from initial state \tilde{x}_r^i .

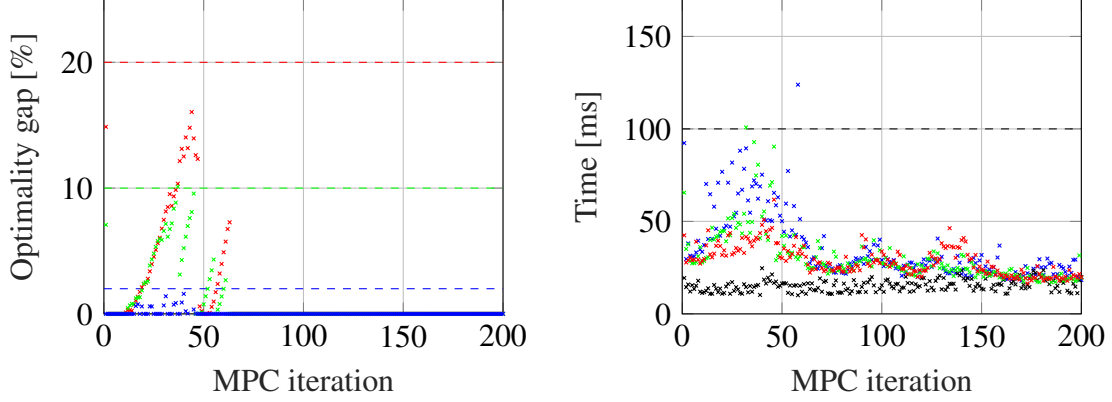


(d) The lateral errors from initial state \tilde{x}_r^i .



(e) The car-like tractor's curvatures from initial state \tilde{x}_r^i .

Figure 10: Simulation results from path following a figure-eight nominal path in $(x_{3r}(\cdot), y_{3r}(\cdot))$ using MIQP-MPC (blue lines), QP-MPC (red lines) and LQ (green lines) from initial state \tilde{x}_r^i in backward motion and from \tilde{x}_f^i in forward motion. In Figure 10a–10b, the initial states for (β_3^i, β_2^i) are marked with black stars. The red dotted and black dotted lines are the trajectories from \tilde{x}_r^i using QP-MPC tuned as in the first set of simulations and using MIQP-MPC with termination criterion $\delta = 0.2$, respectively.



(a) Theoretical (dashed lines) and actual suboptimality gaps (crosses) for each MPC iteration of MIQP-MIQP-MPC. (b) Computation times for each MPC iteration of MIQP-MIQP-MPC.

Figure 11: Computation time and relative suboptimality gap for the MIQP-MPC controller’s first 200 iterations from \tilde{x}_r^i in Figure 9 using the suboptimality gaps: $\delta = 0.02$ (blue crosses), $\delta = 0.1$ (green crosses) and $\delta = 0.2$ (red crosses). In Figure 11b, the black crosses denote the computation time of the QP-MPC controller and the black-dashed line is the controller’s sampling time.

together with its nominal path $(\beta_{3r}(\cdot), \beta_{2r}(\cdot))$ (black solid line). For the forward cases, all controllers are able to converge to the figure-eight nominal path from initial state \tilde{x}_f^i , where the LQ controller converges fastest with no overshoots in the lateral error nor the heading error of the semitrailer (see Figure 9). However, in the LQ case the trajectories for the joint angles (green line in Figure 10b) are exiting the LIDAR-based estimation solution’s sensing region which can cause unsatisfactory behaviors in practice. This is because the used estimation solution is not guaranteed to compute accurate estimates of the semitrailer’s pose nor the joint angles.

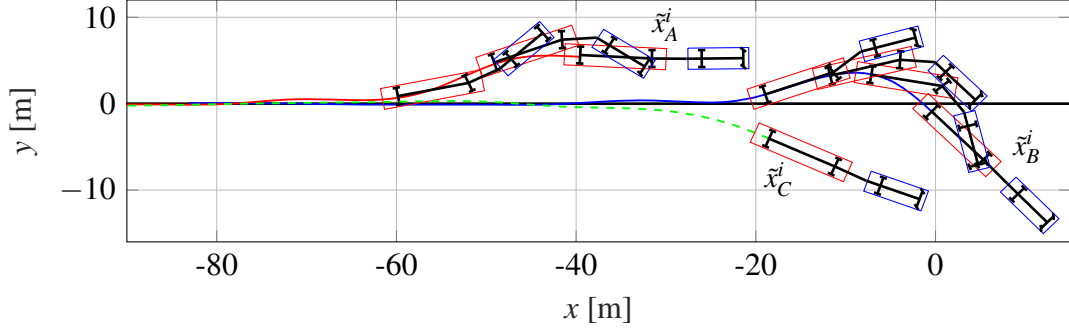
In the simulations, Gurobi’s average computation time for the MIQP-MPC controller is 40 ms (max: 181 ms) in comparison to 17 ms (max: 24 ms) for the QP-MPC controller. That is, the found worst-case computation time for MIQP-MPC is larger than the controller’s specified sampling time of 100 ms. However, global solvers use a fair amount of its computation time only to prove that a found solution satisfies the specified relative suboptimality gap δ . Inspired by the findings in [6], the backward tracking simulation from \tilde{x}_r^i in Figure 9 using MIQP-MPC is repeated by relaxing the MIQP solver’s termination criterion. The computation times and the actual suboptimality gaps for the first 200 MPC iterations (20 seconds) using termination criteria for relative suboptimality gap as $\delta = 0.02$ (blue), $\delta = 0.1$ (green) and $\delta = 0.2$ (red) are presented in Figure 11. From Figure 11b it can be concluded that by selecting $\delta = 0.2$ the worst-case computation time is reduced to 58 ms (mean: 26 ms), on the expense that the

computed control-input sequence is suboptimal at some MPC iterations (see Figure 11a). It is however guaranteed to never be worse than the specified suboptimality gap. Moreover, since the MPC controller operates in a receding horizon fashion, a suboptimal control-input sequence may only have a minor impact on the final trajectory taken by the vehicle. These arguments have strong similarities to well established methods for approximate nonlinear MPC, such as real-time iterations [19]. As an example, the trajectories taken by the vehicle using MIQP-MPC with $\delta = 0.2$ from \tilde{x}_t^i is shown in Figure 10 by black-dotted lines. The results show that the resulting trajectory is almost identical to the one obtained using MIQP-MPC with termination criterion $\delta = 0.02$ (blue lines).

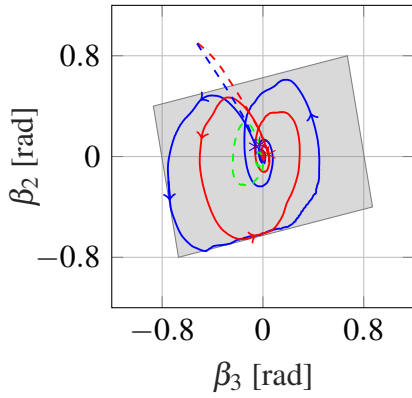
5.3 Field experiments

The QP-MPC controller has been implemented and experimentally validated on a modified version of a Scania R580 6x4 tractor that is shown in Figure 1. The tractor is equipped with additional computation power compared to its commercial version and a servo motor for automated control of its steering column. The tractor is also equipped with a localization system (real-time kinematic GPS [RTK-GPS] and IMUs) and a rear-view LIDAR sensor that is aiming at the semitrailer body (see Figure 6). Neither the semitrailer nor the dolly is equipped with any sensor. Instead the joint angles and the pose of the semitrailer are estimated using an extended Kalman filter (EKF) with the tractor’s pose and virtual measurements of the trailer states as inputs. By running a random sample consensus algorithm [27], the virtual measurements are computed by extracting features of the semitrailer body from the LIDAR’s point cloud. The vehicle parameters are listed in Table 1 and coincide with the ones used in the simulation study. For more details of the test platform, including the LIDAR-based estimation solution, the reader is referred to [27].

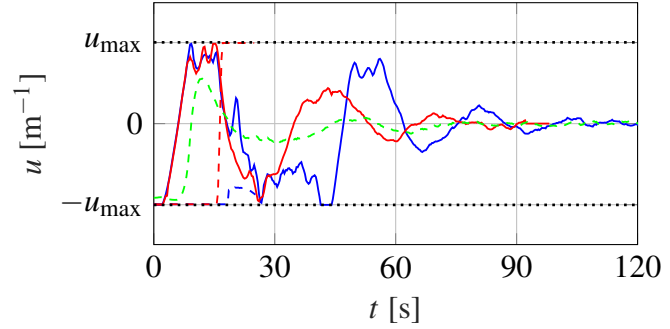
The QP-MPC controller is implemented in C++ and qpOASES [15] is used as QP solver, which is an open-source active-set solver with warm-starts. Based on the results from the tracking of the figure-eight nominal path, the rotated polytope is used to represent the constraint on the joint angles. The controllers are operating in serial with the EKF, where the state estimate \hat{x}_k is used to compute the path-following error \tilde{x}_k at each sampling instance. The performance of the QP-MPC controller is evaluated in a set of real-world experiments of backward tracking a straight and a figure-eight nominal path, where it is also benchmarked with an LQ controller. The design parameters for the controllers are presented in Table 2, which are equal to the ones used in the simulations with the exception that the controller frequency is increased to 20 Hz to meet system architectural constraints.



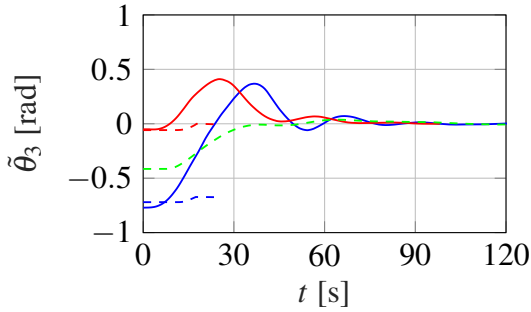
(a) The trajectories taken by the axle of the semitrailer ($x_3(\cdot), y_3(\cdot)$) and the nominal path in ($x_{3r}(\cdot), y_{3r}(\cdot)$) (black solid line).



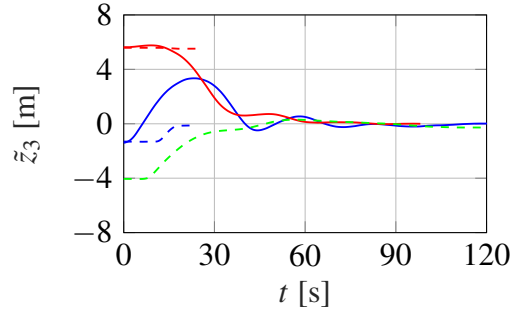
(b) The trajectories for the joint angles where the stars highlight the initial states.



(c) The car-like tractor's curvatures.



(d) The orientation errors of the semitrailer.



(e) The lateral errors of the semitrailer.

Figure 12: Experimental results from path following a straight nominal path ($y_{3r} = 0$) from the three different initial states \tilde{x}_A^i (red), \tilde{x}_B^i (blue) and \tilde{x}_C^i (green) using the QP-MPC controller (solid lines) and the LQ controller (dashed lines).

5.4 Results from field experiments

The QP-MPC controller is first evaluated by tracking a straight nominal path in backward motion ($v = -1$ m/s). As in the simulation study, the initial state $\tilde{x}(0)$ is perturbed (see Figure 12a)

to evaluate how the controllers handle disturbance rejection while satisfying the constraint on the joint angles. In Experiment A, the initial path-following error is $\tilde{x}_A^i = [5.6 \text{ m } 0 \text{ 0 } 0]^T$, in Experiment B the initial error $\tilde{x}_B^i = [-1.2 \text{ m } -0.77 \text{ rad } 0 \text{ 0}]^T$, and in Experiment C the initial path-following error is $\tilde{x}_C^i = [-4.1 \text{ m } -0.42 \text{ rad } 0 \text{ 0}]^T$.

The results from the experiments are presented in Figure 12. In Experiment A and B, the LQ controller is not able to stabilize the tractor-trailer vehicle due to the constraints on the tractor's curvature and jackknifing occurs almost instantly. This can be seen in Figure 12b where the joint-angle trajectories $(\beta_2(\cdot), \beta_3(\cdot))$ are plotted. In contrast to this behavior, the QP-MPC controller is able to make the system converge to the straight nominal path while satisfying the constraints on the joint angles. In experiment C, both controllers are able to stabilize the vehicle around the nominal path. The reason for this can be seen in Figure 12c where the tractor's curvature is plotted. The results show that in Experiment C, the feedback computed by the LQ controller (green dashed line) is not saturating the tractor's curvature, which it does in Experiment A and B.

The second set of experiments involve backward tracking of a figure-eight shaped nominal path in $(x_{3r}(\cdot), y_{3r}(\cdot))$. Also in this set of experiments, the initial path-following error state $\tilde{x}(0)$ is perturbed (see Figure 13) to compare the performance of the controllers. In Experiment D, the initial path-following error is $\tilde{x}_D^i = [3.4 \text{ m } -0.46 \text{ rad } 0.46 \text{ rad } 0.73 \text{ rad}]^T$, in Experiment E the initial error is $\tilde{x}_E^i = [3 \text{ m } 0 \text{ 0.26 rad } 0.27 \text{ rad}]^T$, and in Experiment F the initial error is

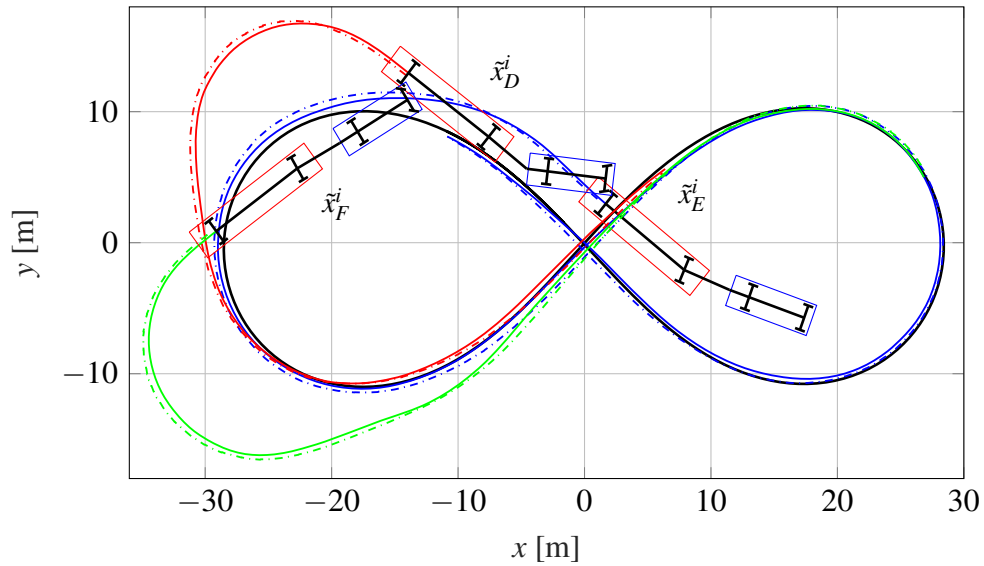
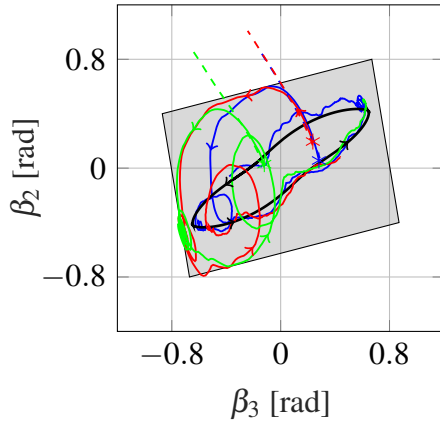
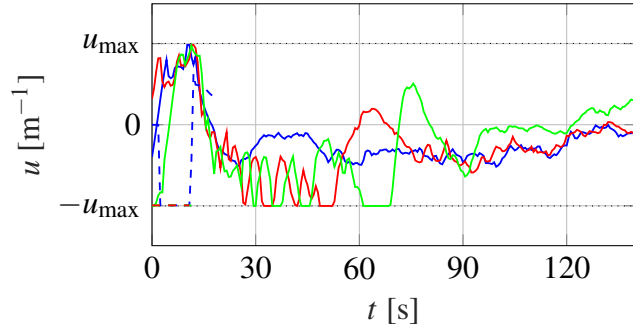


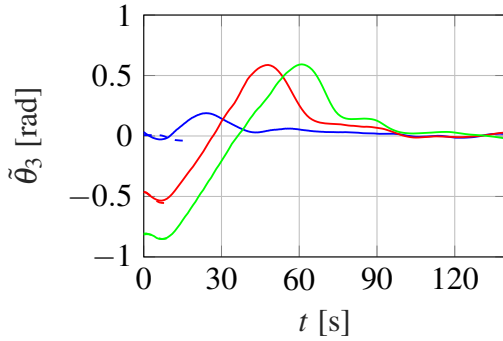
Figure 13: Experimental results from backward tracking a figure-eight nominal path in $(x_{3r}(\cdot), y_{3r}(\cdot))$ (black solid line) from three different initial states \tilde{x}_D^i (red), \tilde{x}_E^i (blue) and \tilde{x}_F^i (green) using the QP-MPC controller (solid lines). The dashed-dotted lines are measured path of the axle of the semitrailer by the external RTK-GPS.



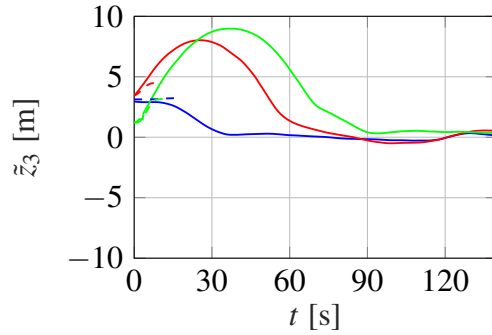
(a) The trajectories for the joint angles where the stars highlight the initial states.



(b) The car-like tractor's curvatures.



(c) The orientation errors of the semitrailer.



(d) The lateral errors of the semitrailer.

Figure 14: Experimental results from backward tracking a figure-eight nominal path in $(x_{3r}(\cdot), y_{3r}(\cdot))$ from three different initial states \tilde{x}_D^i (red), \tilde{x}_E^i (blue) and \tilde{x}_F^i (green) using the QP-MPC controller (solid lines) and the LQ controller (dashed lines). In Figure 14a, the black line is the nominal path in $(\beta_{3r}(\cdot), \beta_{2r}(\cdot))$.

$$\tilde{x}_F^i = [1.2 \text{ m} \quad -0.8 \text{ rad} \quad 0.55 \text{ rad} \quad 0.44 \text{ rad}]^T.$$

The results from the experiments are presented in Figure 13–14. In all three experiments, the LQ controller fails to stabilize the vehicle and jackknifing occurs almost instantly (see Figure 14a). In contrast to this behavior, the QP-MPC controller is able to stabilize the vehicle around the figure-eight nominal path in all three experiments while satisfying the constraints on the joint angles during the majority of the maneuvers. As can be seen in Figure 14a, the joint-angle trajectories for QP-MPC are violating their soft constraints from \tilde{x}_D^i and \tilde{x}_F^i . Even though there are only minor violations, the effect on the linear penalty on constraint violation can be observed in Figure 14b where the tractor's curvature is plotted. Between 25–50 s, there are minor oscillations in the control input which is a result of model errors, small errors in the

joint-angle estimates and the linear cost for violating the soft constraints on the joint angles.

To validate the performance of the used LIDAR-based estimation solution, an external RTK-GPS is mounted on the semitrailer’s axle. As can be seen in Figure 13, even though the maneuvers are advanced the observer is able to track the position of the semitrailer’s axle. One important reason for this is that the QP-MPC controller is restricted to control the vehicle such that its joint angles remain in the region where high-accuracy state estimates can be computed by the used LIDAR-based estimation solution. As a final note, the average computation time for the QP-MPC controller during the experiments was only 5 ms which is an order of magnitude less than the controller’s sampling time of 50 ms.

6 Conclusions and future work

An estimation-aware model predictive path-following control approach for a G2T with a car-like tractor is proposed. The approach targets low-speed maneuvers and is designed to follow nominal paths in forward and backward motion that contain full state and control-input information. The path-following controller is tailored to operate in series with an estimation solution that uses an advanced sensor with a limited FOV to estimate the joint angles and the semitrailer’s pose. To ensure that high-accuracy state estimates can be computed, the estimation solution’s sensing region is modeled as constraints on the joint angles which are included in the MPC formulation. Two modeling approaches are proposed with different computation complexity and performance of the resulting MPC controller. In the first approach that is called MIQP-MPC, the constraints on the joint angles are modeled as a union of convex polytopes, making it necessary to incorporate binary decision variables in the MPC formulation. The second approach is called QP-MPC and avoids binary variables using a single convex polytope leading to a more restrictive approximation of the estimation solution’s sensing region. The proposed MPC approaches are first evaluated in simulations and the QP-MPC is also evaluated in field experiments on a full-scale test vehicle. The computation complexity and performance of the proposed MPC approaches in terms of suppressing disturbances and recovering from non-trivial initial states is benchmarked, and shown to outperform, a previously proposed control strategy where the joint-angle constraints are neglected.

As future work, we would like to investigate if it would be feasible to deploy a suboptimal version of the MIQP-MPC controller on the full-scale test vehicle. This could be done either by relaxing the MIQP solver’s termination criterion or by employing methods for approximate non-linear MPC [19]. We would also like to investigate if there exist other systems with advanced sensors with similar sensing limitations that need to be rigorously respected in the controller.

Acknowledgment

The research leading to these results has been funded by Strategic vehicle research and innovation programme (FFI). The authors gratefully acknowledge the Royal Institute of Technology for providing the external RTK-GPS. The authors would also like to express their gratitude to Scania CV for providing hardware, software and technical support.

Appendix A

The linearization of the path-following error model in (10) around the origin $(\tilde{x}, \tilde{u}) = (0, 0)$ is

$$\frac{d\tilde{x}}{ds} = A(s)\tilde{x} + B(s)\tilde{u}, \quad (31)$$

where the matrices $A(s)$ and $B(s)$ are given by

$$A(s) = \frac{\partial \tilde{f}(s, 0, 0)}{\partial \tilde{x}} = \bar{v}_{3r} \begin{bmatrix} 0 & 1 & 0 & 0 \\ a_{21}(s) & 0 & a_{23}(s) & 0 \\ a_{31}(s) & 0 & a_{33}(s) & a_{34}(s) \\ a_{41}(s) & 0 & a_{43}(s) & a_{44}(s) \end{bmatrix}, \quad (32)$$

and

$$B(s) = \frac{\partial \tilde{f}(s, 0, 0)}{\partial \tilde{u}} = \bar{v}_{3r} \begin{bmatrix} 0 \\ 0 \\ b_3(s) \\ b_4(s) \end{bmatrix}, \quad (33)$$

where

$$\begin{aligned} a_{21}(s) &= -\frac{\tan^2 \beta_{3r}}{L_3^2}, \\ a_{23}(s) &= \frac{1}{L_3 \cos^2 \beta_{3r}}, \\ a_{31}(s) &= \frac{\tan \beta_{3r}(u_r M_1 \cos \beta_{2r} - \sin \beta_{2r})}{L_3 L_2 \cos \beta_{3r} (\cos \beta_{2r} + u_r M_1 \sin \beta_{2r})} + \frac{\tan^2 \beta_{3r}}{L_3^2}, \\ a_{33}(s) &= \frac{\sin \beta_{3r} (\sin \beta_{2r} - u_r M_1 \cos \beta_{2r})}{L_2 \cos \beta_{3r}^2 (\cos \beta_{2r} + u_r M_1 \sin \beta_{2r})} - \frac{1}{\cos^2 \beta_{3r} L_3}, \end{aligned}$$

$$\begin{aligned}
a_{34}(s) &= \frac{1 + u_r^2 M_1^2}{L_2 \cos \beta_{3r} (\cos \beta_{2r} + u_r M_1 \sin \beta_{2r})^2}, \\
a_{41}(s) &= -\frac{\tan \beta_{3r}}{L_2 L_3} \left(\frac{u_r L_2 - \sin \beta_{2r} + M_1 \cos \beta_{2r} u_r}{\cos \beta_{3r} (\cos \beta_{2r} + M_1 u_r \sin \beta_{2r})} \right), \\
a_{43}(s) &= \frac{\tan \beta_{3r}}{L_2} \left(\frac{u_r L_2 + u_r M_1 \cos \beta_{2r} - \sin \beta_{2r}}{\cos \beta_{3r} (\cos \beta_{2r} + u_r M_1 \sin \beta_{2r})} \right), \\
a_{44}(s) &= \frac{1 + u_r^2 M_1^2 + u_r^2 L_2 M_1 \cos \beta_{2r} - u_r L_2 \sin \beta_{2r}}{L_2 \cos \beta_{3r} (\cos \beta_{2r} + u_r M_1 \sin \beta_{2r})^2}, \\
b_3(s) &= -\frac{M_1}{L_2 \cos \beta_{3r} (\cos \beta_{2r} + u_r M_1 \sin \beta_{2r})^2}, \\
b_4(s) &= \frac{M_1 + L_2 \cos \beta_{2r}}{\cos \beta_{3r} L_2 (\cos \beta_{2r} + u_r M_1 \sin \beta_{2r})^2}.
\end{aligned}$$

References

- [1] C. Altafini. Some properties of the general n-trailer. *International Journal of Control*, 74(4):409–424, 2001.
- [2] C. Altafini. Path following with reduced off-tracking for multibody wheeled vehicles. *IEEE Transactions on Control Systems Technology*, 11(4):598–605, 2003.
- [3] C. Altafini, A. Speranzon, and B. Wahlberg. A feedback control scheme for reversing a truck and trailer vehicle. *IEEE Transactions on Robotics and Automation*, 17(6):915–922, Dec 2001.
- [4] D. Arnström. State estimation for truck and trailer systems using deep learning. Master’s thesis, Linköping University, 2018.
- [5] A. Astolfi, P. Bolzern, and A. Locatelli. Path-tracking of a tractor-trailer vehicle along rectilinear and circular paths: A Lyapunov-based approach. *IEEE Transactions on Robotics and Automation*, 20(1):154–160, 2004.
- [6] D. Axehill, T. Besselmann, D. M. Raimondo, and M. Morari. A parametric branch and bound approach to suboptimal explicit hybrid MPC. *Automatica*, 50(1):240–246, 2014.
- [7] E. Balcerak, J. Schikora, P. Wojke, and D. Zobel. Maneuver-based assistance for backing up articulated vehicles. In *Proceeding of the IEEE Conference on Robotics, Automation and Mechatronics, 2004.*, volume 2, pages 1066–1071, 2004.

- [8] P. Bolzern, R. M. DeSantis, A. Locatelli, and D. Masciocchi. Path-tracking for articulated vehicles with off-axle hitching. *IEEE Transactions on Control Systems Technology*, 6(4):515–523, 1998.
- [9] L. Caup, J. Salmen, I. Muharemovic, and S. Houben. Video-based trailer detection and articulation estimation. In *proceedings of the 2013 IEEE Intelligent Vehicles Symposium*, pages 1179–1184, 2013.
- [10] A. W. Divelbiss and J. T. Wen. Trajectory tracking control of a car-trailer system. *IEEE Transactions on Control Systems Technology*, 5(3):269–278, 1997.
- [11] N. Evestedt, O. Ljungqvist, and D. Axehill. Motion planning for a reversing general 2-trailer configuration using Closed-Loop RRT. In *Proceedings of the 2016 IEEE/RSJ International Conference on Intelligent Robots and Systems*, pages 3690–3697, 2016.
- [12] N. Evestedt, O. Ljungqvist, and D. Axehill. Path tracking and stabilization for a reversing general 2-trailer configuration using a cascaded control approach. In *Proceedings of the 2016 IEEE Intelligent Vehicles Symposium*, pages 1156–1161, June 2016.
- [13] P. Falcone, F. Borrelli, J. Asgari, E. H. Tseng, and D. Hrovat. Predictive active steering control for autonomous vehicle systems. *IEEE Transactions on Control Systems Technology*, 15(3):566–580, 2007.
- [14] T. Faulwasser and R. Findeisen. Nonlinear model predictive control for constrained output path following. *IEEE Transactions on Automatic Control*, 61(4):1026–1039, 2015.
- [15] H. J. Ferreau, C. Kirches, A. Potschka, H. G. Bock, and M. Diehl. qpOases: a parametric active-set algorithm for quadratic programming. *Mathematical Programming Computation*, 6(4):327–363, Dec 2014.
- [16] C. F. Garcia, D. M. Prett, and M. Morari. Model predictive control: theory and practice a survey. *Automatica*, 25(3):335–348, 1989.
- [17] L. Gurobi Optimization. Gurobi Optimizer Reference Manual, 2019.
- [18] M. Hafner and T. Pilutti. Control for automated trailer backup. Technical report, SAE Technical Paper, 2017.
- [19] B. Houska, H. J. Ferreau, and M. Diehl. An auto-generated real-time iteration algorithm for nonlinear MPC in the microsecond range. *Automatica*, 47(10):2279 – 2285, 2011.
- [20] IBM. CPLEX, 2020.

- [21] E. Kayacan, E. Kayacan, H. Ramon, and W. Saeys. Robust tube-based decentralized nonlinear model predictive control of an autonomous tractor-trailer system. *IEEE Transactions on Mechatronics*, 20(1):447–456, 2014.
- [22] F. Lamiroux, S. Sekhavat, and J. P. Laumond. Motion planning and control for hilare pulling a trailer. *IEEE Transactions on Robotics and Automation*, 15(4):640–652, Aug 1999.
- [23] B. Li, T. Acarma, Y. Zhang, L. Zhang, C. Yaman, and Q. Kong. Tractor-trailer vehicle trajectory planning in narrow environments with a progressively constrained optimal control approach. *IEEE Transactions on Intelligent Vehicles*, 2019.
- [24] P. F. Lima, M. Nilsson, M. Trincavelli, J. Mårtensson, and B. Wahlberg. Spatial model predictive control for smooth and accurate steering of an autonomous truck. *IEEE Transactions on Intelligent Vehicles*, 2(4):238–250, Dec 2017.
- [25] X. Liu and D. Cebon. A minimum swept path control strategy for reversing articulated vehicles. In *Proceedings of the 2018 IEEE Intelligent Vehicles Symposium*, pages 1962–1967, June 2018.
- [26] O. Ljungqvist, D. Axehill, and H. Pettersson. On sensing-aware model predictive path-following control for a reversing general 2-trailer with a car-like tractor. *Accepted to Proceedings of the 2020 IEEE International Conference on Robotics and Automation (ICRA)*. Pre-print: <https://arxiv.org/abs/2002.06874>, 2020.
- [27] O. Ljungqvist, N. Evestedt, D. Axehill, M. Cirillo, and H. Pettersson. A path planning and path-following control framework for a general 2-trailer with a car-like tractor. *Journal of Field Robotics*, 36(8):1345–1377, 2019.
- [28] J. Löfberg. YALMIP: A toolbox for modeling and optimization in MATLAB. In *Proceedings of the 2004 IEEE International Symposium on Computer Aided Control Systems Design*, pages 284–289, 2004.
- [29] D. Q. Mayne, J. B. Rawlings, C. V. Rao, and P. O. Scokaert. Constrained model predictive control: Stability and optimality. *Automatica*, 36(6):789–814, 2000.
- [30] M. M. Michaek. A highly scalable path-following controller for n-trailers with off-axle hitching. *Control Engineering Practice*, 29:61–73, 2014.
- [31] M. M. Michaek. Cascade-like modular tracking controller for non-standard n-trailers. *IEEE Transactions on Control Systems Technology*, 25(2):619–627, March 2017.

- [32] M. Michałek and M. Kielczewski. Helping a driver in backward docking with N-trailer vehicles by the passive control-assistance system. In *Proceeding of the 16th International IEEE Conference on Intelligent Transportation Systems*, pages 1993–1999, 2013.
- [33] M. Michałek and M. Kielczewski. The concept of passive control assistance for docking maneuvers with N-trailer vehicles. *IEEE/ASME Transactions on Mechatronics*, 20(5):2075–2084, 2014.
- [34] M. M. Michalek. Cascaded approach to the path-following problem for n-trailer robots. In *9th International Workshop on Robot Motion and Control*, pages 161–166, July 2013.
- [35] M. M. Michalek. Non-minimum-phase property of n-trailer kinematics resulting from off-axle interconnections. *International Journal of Control*, 86(4):740–758, 2013.
- [36] M. M. Michałek and D. Pazderski. Forward tracking of complex trajectories with non-standard n-trailers of non-minimum-phase kinematics avoiding a jackknife effect. *International Journal of Control*, pages 1–14, 2018.
- [37] J. Morales, J. L. Martinez, A. Mandow, and A. J. Garcia-Cerezo. Steering the last trailer as a virtual tractor for reversing vehicles with passive on- and off-axle hitches. *IEEE Transactions on Industrial Electronics*, 60(12):5729–5736, Dec 2013.
- [38] P. Nyberg. Stabilization, sensor fusion and path following for autonomous reversing of a full-scale truck and trailer system. Master’s thesis, Linköping University, 2016.
- [39] C. Pradalier and K. Usher. Robust trajectory tracking for a reversing tractor trailer. *Journal of Field Robotics*, 25(6-7):378–399, 2008.
- [40] A. J. Rimmer and D. Cebon. Implementation of reversing control on a doubly articulated vehicle. *Journal of Dynamic Systems, Measurement, and Control*, 139(6):061011, 2017.
- [41] M. Sampei and K. Furuta. On time scaling for nonlinear systems: Application to linearization. *IEEE Transactions on Automatic Control*, 31(5):459–462, 1986.
- [42] M. Sampei, T. Tamura, T. Kobayashi, and N. Shibui. Arbitrary path tracking control of articulated vehicles using nonlinear control theory. *IEEE Transactions on Control Systems Technology*, 3(1):125–131, 1995.
- [43] C. Samson. Control of chained systems application to path following and time-varying point-stabilization of mobile robots. *IEEE Transactions on Automatic Control*, 40(1):64–77, Jan 1995.

- [44] C. D. Saxe and D. Cebon. A visual template-matching method for articulation angle measurement. In *proceedings of the 2015 IEEE 18th International Conference on Intelligent Transportation Systems*, pages 626–631, Sept 2015.
- [45] O. J. Sjørdalen. Conversion of the kinematics of a car with n trailers into a chained form. In *Proceedings of the 1993 IEEE International Conference on Robotics and Automation*, pages 382–387. IEEE, 1993.
- [46] M. Werling, P. Reinisch, M. Heidingsfeld, and K. Gresser. Reversing the general one-trailer system: Asymptotic curvature stabilization and path tracking. *IEEE Transactions on Intelligent Transportation Systems*, 15(2):627–636, 2014.
- [47] P. H. Williams. *Model building in mathematical programming*. John Wiley & Sons, 2013.